A Flux-Limited Numerical Method for the MHD Equations to Simulate Propulsive Plasma Flows *

K. Sankaran†, **L. Martinelli**‡ and **E.Y. Choueiri**§
Mechanical and Aerospace Engineering Department
Princeton University, Princeton, New Jersey 08544

AIAA-2000-2350¶

June 19, 2000

Abstract

For numerical simulations to be effective tools in plasma propulsion research, a higher order accurate solver that captures MHD shocks monotonically and works reliably for strong magnetic fields is needed. For this purpose, a characteristics based scheme for the MHD equations, with flux limiters to improve spatial accuracy, has been developed. In this method, the symmetric form of the MHD equations, accounting for waves propagating in all directions, is solved. The required eigensystem of axisymmetric MHD equations, with appropriate normalization, is presented. This scheme was validated against unsteady (Riemann problem) and force-free equilibrium (Taylor state) test cases. The capability of this method to simulate resistive plasma flows is demonstrated using a simple example.

1 Introduction

Plasma propulsion systems offer significantly higher exhaust velocities than chemical propulsion systems, and process more power and produce higher thrust densities than space-charge limited electric propulsion systems, as seen in figs.(1), (2). The fundamental acceleration process involves converting electrical energy into kinetic energy of the propellant, by the application of electromagnetic body forces. However, this simple explanation belies the complexity of the electromagnetic acceleration processes, which embodies interlocking aspects of compressible gasdynamics, ionized gas physics, electromagnetic field theory, particle electrodynamics (as explained in ref.[1]) and plasma-surface interactions (ref.[2]). The resulting theoretical complexity makes realistic description of the flow analytically intractable.

As shown in Fig.(3), the electrical power deposited into the plasma can be expended into many sinks, only two of which, directed electromagnetic kinetic power and directed electrothermal kinetic power, are useful for propulsion. Understanding and quantifying these disparate processes is essential to improving the efficiency of these devices. Since it is difficult to do so using an empirical approach, numerical simulations are valuable tools in plasma thruster research. Moreover, simulations can be valuable aides to expensive, and sometimes impractical, experimental parametric studies.

2 Plasma Thruster Simulations

The importance of numerical simulation in advancing plasma thruster research was realized early in its history. Martinache[5] and Villani[6] at Princeton made some of the earlier attempts to use simple computer codes to study these devices. Later, Kimura[7] *et al.* at Institute of Space and Astronautical Sciences, and Fujiwara[8] at Nagoya University, started developing single-temperature, 2-D models on simple geome-

*Research supported by NASA-JPL's Advanced Propulsion Group.

†Graduate Student, Research Assistant. Member AIAA.

‡Associate Professor, Associate Fellow AIAA.

§Chief Scientist at EPPDyL. Assistant Professor, Applied Physics Group. Senior Member AIAA.

¶Presented at the 31st Plasmadynamics and Lasers Conference, Denver, CO, June 19-22, 2000.

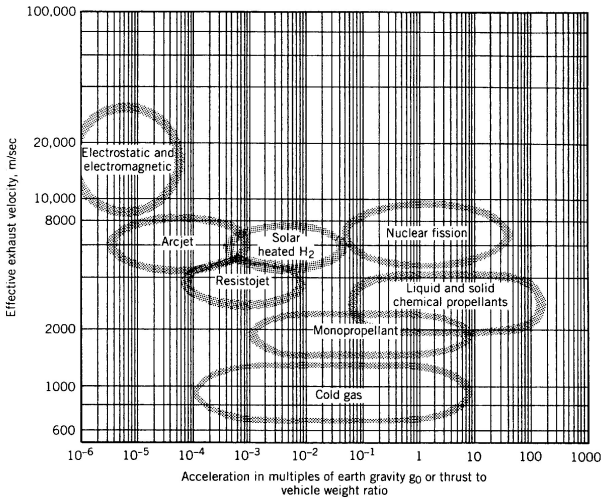

Figure 1: Realm of electric propulsion among other space propulsion systems (from ref.[3]).

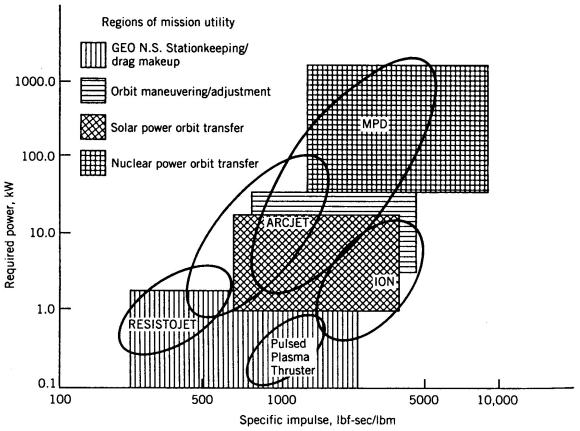

Figure 2: Realm of electromagnetic accelerators among other electric propulsion systems (from ref.[3]).

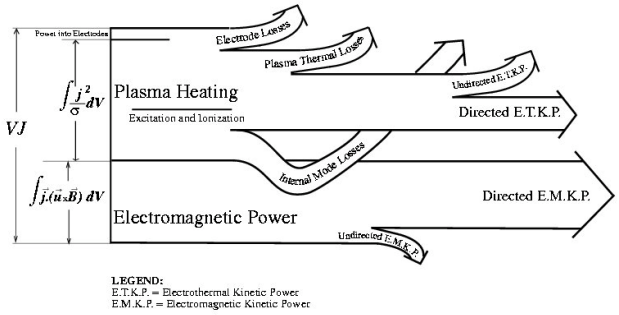

Figure 3: Expenditure of input power in an electromagnetic accelerator (not to scale, from ref.[4]).

tries, and have continued to make improvements to their models. Currently, the efforts of Fujiwara[9] *et al.* are directed at studying critical phenomena in magnetoplasmadynamic thrusters (MPDT), using multi-temperature models. Caldo and Choueiri[10] at Princeton have developed a two-temperature model to study the effects of anomalous transport, described in ref.[11], on MPD flows. The effort by LaPointe[12] focused on studying the effect of geometry on performance. Martinez-Sanchez[13],[14] *et al.* at MIT have developed multi-temperature axisymmetric numerical models to study various aspects of the flow. Turchi[15] *et al.* at Ohio State use MACH2, an unsteady MHD solver developed for high power plasma gun simulation, to model PPTs and MPD thrusters in many geometries. MACH3[16], the next generation of MACH2, is also used to simulate possible 3-D effects in specific situations. The most persistent effort so far has been that of Sleziona[17],[18] *et al.* at University of Stuttgart, who have been developing numerical models for MPD thrusters for over a decade. Detailed models for many transport processes and multiple levels of ionization have been incorporated into their governing equations, which are solved on unstructured adaptive grids.

Despite these efforts, there remains a need for accurate and robust numerical schemes to simulate propulsive plasma flows. In general, three shortcomings of existing models can be identified.

1. Some of the above mentioned codes exhibit numerical instabilities at high current levels. MPD thrusters perform better at higher currents, and many of the important research questions, such as performance limiting phenomena, tend to also occur at higher currents. Consequently, the inability of a simulation to work reliably at those situations undermines its value.

   A probable explanation for these instabilities is the failure to solve the magnetic field evolution self-consistently with the flow. For highly resistive flows, the time scale for resistive diffusion of the magnetic field is orders of magnitude smaller than that of convection. However, in MPD flows it is common to have resistivities of $\mathcal{O}(10^{-4})$ Ohm.m. In such situations, these time

scales are not very far off, and there is a strong coupling between the flow and the magnetic field. The corresponding magnetic Reynolds' numbers indicate that both convective and resistive diffusion of the magnetic field are important. Moreover, the Alfvèn and fluid time scales are not very disparate. Therefore, the full set of equations describing the flow field and magnetic field evolution have to be computed self-consistently.

An important feature of the MHD formalism is the multitude of waves it permits to exist. The nonlinear coupling of these waves play an important role in determining physical phenomena and in computing the solution, as explained in ref.[19]. Solving Maxwell's equations consistently with compressible gasdynamics equations naturally produces waves physically associated with the problem, such as Alfvèn and magnetosonic waves, as eigenvalues. Such a formulation is thus suitable for handling MHD waves and shocks.

2. Some of the earlier efforts have experienced problems conserving mass, momentum, and energy. A conservative formulation of the governing equations ensures that these quantities are indeed conserved. Such a formulation also facilitates the application of boundary conditions, since the fluxes are the only quantities to be specified at the boundaries. From the perspective of numerical solution, it can be shown that conservative formulation is necessary for accurately capturing discontinuities.

3. Though noted earlier (ref.[14]), none of the existing models (with the exception of recent work ref.[18]) take advantage of the developments in the techniques for numerical solution of Euler and Navier-Stokes equations. These techniques allow non-oscillatory capturing of shocks and high accuracies in smooth regions of the flow.

For the reasons explained above, the numerical scheme developed in this work has three salient features:

1. Self-consistent treatment of flow and magnetic field equations,

2. Conservative formulation of the problem,

3. Characteristics-splitting techniques satisfying Rankine-Hugoniot relations, combined with anti-diffusion to increase accuracy.

The solver developed based on these principles will be described in the following sections.

3 MHD Equations

The solver developed in this work can be illustrated with the simple flow problem of a fully ionized, quasi-neutral plasma in thermal equilibrium under conditions for which the continuum treatment is valid. Subsequent physical models can be added as deemed appropriate, without significant changes to the underlying numerical building blocks of the solver. The governing equations for this problem can be written in the form:

$$\frac{\partial}{\partial t}\begin{bmatrix}\rho\\ \rho\mathbf{u}\\ \mathbf{B}\\ \mathcal{E}\end{bmatrix}+\nabla\cdot\begin{bmatrix}\rho\mathbf{u}\\ \rho\mathbf{u}\mathbf{u}+\bar{\bar{\mathrm{p}}}-\bar{\bar{\mathcal{B}}}_M\\ \mathbf{u}\mathbf{B}-\mathbf{B}\mathbf{u}\\ (\mathcal{E}+p)\,\mathbf{u}-\bar{\bar{\mathcal{B}}}_M\cdot\mathbf{u}\end{bmatrix}=\mathbf{S}. \quad (1)$$

The vector of source terms, $\mathbf{S}$, contains contributions due to round-off errors in $\nabla\cdot\mathbf{B}$, and physical dissipative effects:

$$\mathbf{S}_{\nabla\cdot\mathbf{B}}=(\nabla\cdot\mathbf{B})\begin{bmatrix}0\\ \frac{\mathbf{B}}{\mu_o}\\ \mathbf{u}\\ \frac{\mathbf{B}}{\mu_o}\cdot\mathbf{u}\end{bmatrix},\ \mathbf{S}_{dis}=\nabla\cdot\begin{bmatrix}0\\ \bar{\bar{\tau}}_{vis}\\ \bar{\bar{E}}_{res}\\ \mathbf{q}\end{bmatrix}. \quad (2)$$

The continuity equation does not have any source or sink terms because this model assumes complete ionization and no recombination, and the nuclei are neither created nor destroyed.

The momentum equation contains the electromagnetic body force per unit volume, $\mathbf{j}\times\mathbf{B}$, written as the divergence of the Maxwell stress tensor $\bar{\bar{\mathcal{B}}}_M$, as described in ref.[1]. Here, $\bar{\bar{p}}$ is the isotropic thermodynamic pressure tensor, and $\bar{\bar{\tau}}_{vis}$ is the viscous stress tensor.

In Faraday's law, the convective diffusion of the magnetic field, which is the contribution of the back EMF, is written as a divergence of the antisymmetric tensor $\mathbf{u}\mathbf{B}-\mathbf{B}\mathbf{u}$. The resistive diffusion appears as divergence of the resistive diffusion tensor, $\bar{\bar{E}}_{res}$, as in ref.[20],

$$\nabla\cdot\bar{\bar{E}}_{res}=-\nabla\times\left[\bar{\bar{\eta}}\cdot\frac{\nabla\times\mathbf{B}}{\mu_o}\right],$$

where $\bar{\bar{\eta}}$ is the full resistivity tensor, which includes the dispersive Hall effect.

The energy equation is written in terms of the energy density (energy per unit volume), $\mathcal{E}$, whose components are the internal energy, kinetic energy and the energy in the magnetic field:

$$\mathcal{E} = \frac{p}{\gamma - 1} + \frac{1}{2}\rho \mathbf{u}\cdot\mathbf{u} + \frac{\mathbf{B}\cdot\mathbf{B}}{2\mu_o} \ .$$

Apart from the familiar convective flux of energy, $(\mathcal{E}+p)\,\mathbf{u}$, the other terms are the energy expended in electromagnetic acceleration, $\bar{\bar{\mathcal{B}}}_M \cdot \mathbf{u}$, and the energy sources/sinks due to viscous heating, Ohmic heating, and thermal conduction,

$$\nabla\cdot\mathbf{q} = \nabla\cdot\left[\{\bar{\bar{\tau}}_{vis}\cdot\mathbf{u}\} + \left\{\frac{\mathbf{B}\times(\bar{\bar{\eta}}\cdot\mathbf{j})}{\mu_0}\right\} + \{\bar{\bar{\kappa}}\cdot\nabla T\}\right].$$

Under some physical conditions, when the magnetic pressure is several orders of magnitude larger than thermodynamic pressure, the conservation form of the energy equation may not be suitable. In these cases, since the thermodynamic pressure, p, is calculated by subtracting one large number ($B^2/2\mu_o$) from another ($\mathcal{E}$), the associated errors could be large. However, for the conditions that are of interest to plasma propulsion, the magnetic pressure is seldom two orders of magnitude greater than thermodynamic pressure. Thus the conservation form of the energy equation is numerically suitable here.

The treatment of the $\nabla\cdot\mathbf{B}$ terms are important, since they could be a cause of numerical instabilities, as explained in ref.[21]. The technique of Powell[22] to absorb these terms into the Jacobian ensures that any artificial source is convected away as,

$$\frac{\partial}{\partial t}(\nabla\cdot\mathbf{B}) + \nabla\cdot(\mathbf{u}\nabla\cdot\mathbf{B}) = 0. \qquad (3)$$

Since the physical dissipation is written in the divergence form, the entire set of equations can be written in the form,

$$\frac{\partial\mathbf{U}}{\partial t} + \nabla\cdot\mathcal{F}_{conv} = \nabla\cdot\mathcal{F}_{diff} \ , \qquad (4)$$

where $\bar{\bar{\mathcal{F}}}_{conv}$ is the convective flux tensor, and $\bar{\bar{\mathcal{F}}}_{dis}$ the dissipative flux tensor.

4 Numerical Solution

The emphasis of this paper is on the numerical techniques for the hyperbolic nature of the convective part of the problem. One reason for this is that the goal of this work is to simulate problems in propulsion and therefore computing the flow is the most important part. More importantly, it is this part of the problem that has required improvements. The dissipative part of the problem, which brings in a parabolic nature to the governing equations, is relatively well understood. However, as explained in section 2, there is strong coupling between the hyperbolic and the parabolic part of the problem. This coupling raises important issues in spatial as well as temporal discretization, which will be discussed in this section.

4.1 Mesh System

Before delving into the details of numerical solution, a choice of mesh system has to be made. For the cylindrical coordinate system that is most suitable to study many plasma thrusters, the easiest choice is to use structured grids where the finite volumes are concentric shells. Apart from their simplicity, they are also computationally inexpensive. However, they impose a limitation on the variety of geometries that can be modeled.

The use of unstructured grids to simulate plasma thrusters has gained some popularity (ref.[17], [18]). Though the obvious advantage is the freedom to specify an arbitrary geometry, there are some disadvantages that may not be immediately apparent. Unstructured grids are computationally expensive and there are problems in extending higher order accurate schemes to them. Since precise control of geometry may not be as critical to the design of plasma thrusters as it is to, say aircraft design, the use of unstructured grids may not be as crucial.

A good settlement in this issue would be to use body-fitted meshes, and maintain the use of higher order accurate schemes. Work is underway to implement this solver on such a meshing system.

The variables to be computed, given by $\mathbf{U}$ in eqn.(4), can be stored either in the vertices of the cells, or in the center of the cells (ref.[23]). In the former, the variables will coincide with the boundary, and they will be specified as boundary conditions. In the latter, the faces of the cells will be aligned with the walls, and the fluxes of these variables will be specified as boundary conditions. While solving the conservative formulation, it is preferable to choose the cell-centered scheme since specifying the fluxes is more compatible with the governing equations.

4.2 Spatial Discretization

Discretization of a mixed set of equations has to be done prudently. Simple explicit central differencing schemes are well suited for parabolic problems, but ill suited for hyperbolic problems. Conversely, simple explicit backward differencing schemes are well suited for hyperbolic problems, but ill suited for parabolic problems. The discretization method used for both these cases will be addressed.

The numerical solution of the set of hyperbolic equations is based on techniques that are extensively used in computational fluid dynamics. The principles underlying the design of non-oscillatory discretization schemes for compressible flows have been well established over the past decade. There are two important issues in the design of discretization schemes:

- Estimating the numerical flux through cell boundaries, and accounting for waves propagating at different speeds, and possibly in different directions,
- Obtaining non-oscillatory solutions and capturing discontinuities with sufficient accuracy.

The numerical scheme used in this work is derived from research based on the pioneering work of Godunov [24], [25]. The characteristics-splitting technique, which will be described later, was first developed (ref.[26], [27]) to solve problems in compressible fluid dynamics, and has been proven to work reliably in the solution of Navier-Stokes equations.

Analyzing stability and convergence of a nonlinear set of equations is a nontrivial task. The most popular check used is the TVD principle. A practical limitation of the TVD condition is that its extension to multidimensional problems does not provide a satisfactory measure of oscillations. The concept of local extremum diminishing (LED) schemes, developed by Jameson[28], can be extended to multiple dimensions, and ensures that there are no unbounded local oscillations. It has been shown (ref.[28]) that TVD is in fact a 1-D special case of the LED framework. These schemes can be combined with flux limited anti-diffusion to provide higher order accuracy in smooth regions of the flow. These concepts are explained in the ensuing section.

Numerical methods for parabolic problems are relatively commonplace. The equations dictate that the numerical scheme should be second-order accurate in space. In the framework used here, this implies that the first derivatives of variables are to be known across the cell faces. A good way to achieve this has been adapted from an earlier work (ref.[23]), and is illustrated in Fig.(4). The gradient across a cell face is an algebraic average of the value of the gradient at the cell vertex. The vertex value is calculated using discrete Stokes theorem in the shaded area. The net diffusive flux is is estimated from gradients across the adjacent faces.

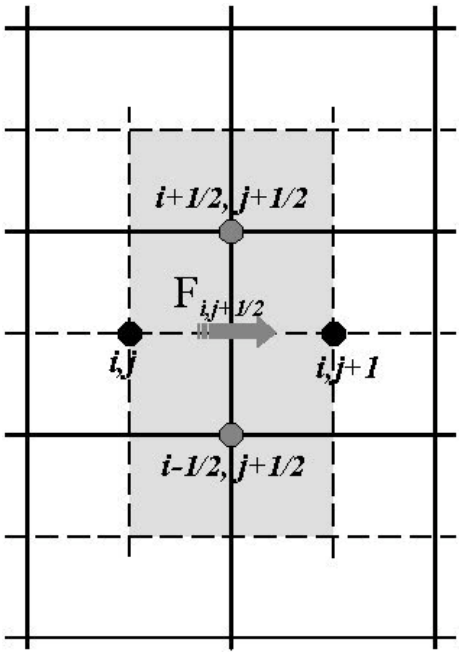

Figure 4: Discretization for diffusion equations

4.3 Temporal Discretization

Unlike in fluid mechanics, the equations of MHD allow many different types of waves to exist. Even though physically the flow velocity is the sought quantity of most interest to propulsion, numerically the velocity of the fastest wave is what determines the time-step constraints. In plasmas of propulsion interest, the fluid velocity is $\mathcal{O}(10^4)$ m/s . For a quasineutral plasma with charge density of $\mathcal{O}(10^{21})/\mathrm{m}^3$ and thermodynamic pressures of $\mathcal{O}(10^{-1})$ Torr and magnetic pressure of $\mathcal{O}(10^1)$ Torr, the fast magnetosonic wave speed is typically of the same order of magnitude as the flow velocity. This indicates that an explicit time marching scheme is suitable. From the CFL criterion, the time step for such a problem would be $\mathcal{O}(10^{-8} - 10^{-9})$ s.

A multi-stage scheme can be chosen to march for-

ward in time. Writing eqn.(1) as,

$$\frac{d\mathbf{U}}{dt} + \mathcal{F}(\mathbf{U}) = 0 \ , \tag{5}$$

where $\mathcal{F}(\mathbf{U})$ represents the sum of all the fluxes, the multi-stage scheme can be written as:

$$\begin{array}{ll} \mathbf{U}^1 & = \mathbf{U}^n - \alpha_1 \Delta t \ \mathcal{F}\left(\mathbf{U}^n\right) \ , \\ \mathbf{U}^2 & = \mathbf{U}^n - \alpha_2 \Delta t \ \mathcal{F}\left(\mathbf{U}^1\right) \ , \\ \mathbf{U}^3 & = \mathbf{U}^n - \alpha_3 \Delta t \ \mathcal{F}\left(\mathbf{U}^2\right) \ , \\ \mathbf{U}^4 & = \mathbf{U}^n - \alpha_4 \Delta t \ \mathcal{F}\left(\mathbf{U}^3\right) \ , \\ \mathbf{U}^{n+1} & = \mathbf{U}^4 \ . \end{array} \tag{6}$$

The coefficients are $\alpha_1 = 0.1084, \alpha_2 = 0.2602, \alpha_3 = 0.5052, \alpha_4 = 1.0$, and the scheme is fourth order accurate in time.

Physical dissipation brings in different characteristic time scales into the problem. They are:

Viscous diffusion:	$= \rho \Delta r^2 / \mu_{visc}$	$\sim 10^{-9}$ s
Magnetic diffusion:	$= \mu_o \Delta r^2 / \eta$	$\sim 10^{-10}$ s
Heat conduction:	$= n_e k_B \Delta r^2 / \kappa_{th}$	$\sim 10^{-9}$ s

If these were vastly different, that would call for an implicit treatment of time stepping. That is not the case here, and an explicit time-stepping scheme was chosen.

Depending upon the particular case being simulated, the difference between convective and dissipative time scales could be more severe. Then, evaluating the convective fluxes at the time scales of dissipative fluxes would be prohibitively expensive. In order to side step this difficulty, a sub-stepping scheme can be chosen. In this method, the convective fluxes are evaluated using a time step based on the CFL limit for the hyperbolic problem, and an intermediate solution is obtained. This intermediate ideal MHD solution is used to advance the parabolic problem, using the diffusive time step limits, to obtain the complete solution at a time $t + \Delta t$.

5 Solution of Ideal MHD

5.1 Characteristics-Splitting Method

Any time-dependent conservation law, such as eqn.(1), can be written in a general form:

$$\frac{d\mathbf{U}_j}{dt} = \sum_{j \neq k} C_{j,k} \left(\mathbf{U}_k - \mathbf{U}_j\right). \tag{7}$$

If the numerical scheme has a compact stencil in which the value at a point is directly dependent only on its nearest neighbors, and if the coefficients are all non-negative, then:

$$C_{j,k} = \begin{cases} \geq 0; k = j \pm 1, \\ = 0; \text{else} \end{cases} \tag{8}$$

If $\mathbf{U}_j$ is a local maximum, then, $(\mathbf{U}_k - \mathbf{U}_j) \leq 0$, causing $\frac{d\mathbf{U}_j}{dt} \leq 0$. Conversely, if $\mathbf{U}_j$ is a local minimum, then, $(\mathbf{U}_k - \mathbf{U}_j) \geq 0$, causing $\frac{d\mathbf{U}_j}{dt} \geq 0$. In other words, this scheme is local extremum diminishing. Apart from ensuring that there are no local oscillations, a scheme built on these conditions can be easily extended to multi dimensions, which was a drawback of the TVD concept.

It has been shown (ref.[28]) that schemes built on obtaining information from the upwind part of a characteristic satisfy positivity constraints (eqn.(8)) and are thus stable. This concept is used in the developing the numerical scheme used in this work.

The method can be explained using eqn.(1) in 1-spatial dimension,

$$\frac{d\mathbf{U}_j}{dt} + \frac{\mathbf{Hz}_{j+\frac{1}{2}} - \mathbf{Hz}_{j-\frac{1}{2}}}{\Delta z} = 0, \tag{9}$$

where $\mathbf{U}$ is the vector of conserved variables, $\mathbf{Hz}$ is the approximation of flux in the $\hat{z}$ direction.

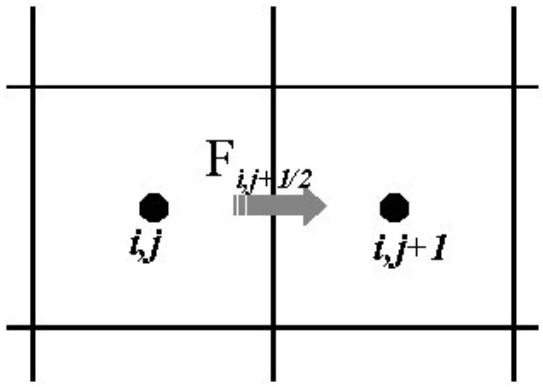

Figure 5: Discretization for convection equations

The true flux, shown in Fig.(5), obtained from eqn.(1), in the $\hat{z}$ direction can be split as,

$$\mathbf{Fz}(\mathbf{U}) = \mathbf{Fz}(\mathbf{U})^+ + \mathbf{Fz}(\mathbf{U})^-, \tag{10}$$

where the eigenvalues of $d\mathbf{Fz}^+/d\mathbf{U}$ are all non-negative, and the eigenvalues of $d\mathbf{Fz}^-/d\mathbf{U}$ are all

non-positive. Then, the approximation of flux is estimated as,

$$\mathbf{Hz}_{j+\frac{1}{2}} = \mathbf{Fz}_j^+ + \mathbf{Fz}_{j+1}^-.$$

Using eqn.(10), this can be rewritten as,

$$\mathbf{Hz}_{j+\frac{1}{2}} = \frac{1}{2}\left(\mathbf{Fz}_j + \mathbf{Fz}_{j+1}\right) - \mathbf{Dz}_{j+\frac{1}{2}},$$

where

$$\mathbf{Dz}_{j+\frac{1}{2}} = \frac{1}{2}\left[\left\{\mathbf{Fz}_{j+1}^+ - \mathbf{Fz}_j^+\right\} + \left\{\mathbf{Fz}_{j+1}^- - \mathbf{Fz}_j^-\right\}\right]. \quad (11)$$

There still remains a question of how $\mathbf{Fz}^+$ and $\mathbf{Fz}^-$ can be evaluated. This evaluation is possible if there is a matrix $\mathbf{A}$, such that

$$\mathbf{Fz}_{j+1} - \mathbf{Fz}_j = \mathbf{A}\cdot\left(\mathbf{U}_{j+1} - \mathbf{U}_j\right). \quad (12)$$

Note that, in the case the points $j+1$ and j are on opposite sides of a discontinuity, eqn.(12) indicates that this scheme satisfies the Rankine-Hugoniot jump conditions exactly.

For a hyperbolic system of equations, $\mathbf{A}$ can be diagonalized as:

$$\mathbf{A} \equiv \mathbf{R}\mathbf{\Lambda}\mathbf{R}^{-\mathbf{1}}, \quad (13)$$

where $\mathbf{R}$ contains the right eigenvectors of $\mathbf{A}$ as its columns, and $\mathbf{R}^{-1}$ contains the left eigenvectors of $\mathbf{A}$ as its rows. $\mathbf{\Lambda}$ is the diagonal matrix of eigenvalues of $\mathbf{A}$. Since $\mathbf{\Lambda}$ can be easily split into,

$$\mathbf{\Lambda} = \mathbf{\Lambda}^+ + \mathbf{\Lambda}^-,$$

using eqn.(13), $\mathbf{A}$ can be split. Thus if there exists an $\mathbf{A}$ such that eqn.(12) is true, then $\mathbf{F}$ can be split. For the Euler equations, this matrix was derived by Roe[26], [27]. There have been efforts by Cargo[29] and Powell[30] to derive such matrices for MHD equations. The literature[31] suggests that various forms of averaged matrices work satisfactorily.

From Godunov's theorem[24], it is evident that the scheme can only be first order accurate. However, away from the discontinuities, the spatial accuracy of the scheme can be improved by including flux-limited anti-diffusion, as described in ref.[28]:

$$\mathbf{Dz}_{j+\frac{1}{2}} = \frac{1}{2}\left|\mathbf{A}\right|\left[\Delta\mathbf{U}_{j+\frac{1}{2}} - \mathbf{Lz}\left(\Delta\mathbf{U}_{j+\frac{3}{2}}, \Delta\mathbf{U}_{j-\frac{1}{2}}\right)\right]. \quad (14)$$

Similar equations can be written for the corresponding terms in the $\hat{r}$ direction.

An alternative to characteristics-splitting for solving conservation form of the equations is to use scalar diffusion. In this formalism, the equivalent expression for eqn.(11) is,

$$\mathbf{Dz}_{j+\frac{1}{2}} = \frac{1}{2}\left|\lambda\right|_{max}\Delta\mathbf{U}_{j+\frac{1}{2}}. \quad (15)$$

Because of its low computational cost, scalar diffusion schemes such as eqn.(15) have been successfully adapted for many commercial applications. However, as described in ref.[28], these schemes tend to artificially smooth out the solution.

5.2 Validation of the Scheme

5.2.1 Unsteady Case

The test problem chosen was of the classical Riemann type, which consists of a single jump discontinuity in an otherwise smooth initial conditions. In 1-D the problem is:

$$\mathbf{U}(x,0) = \begin{cases} \mathbf{U}_L & \text{if } x < \frac{L}{2} \\ \mathbf{U}_R & \text{if } x \geq \frac{L}{2} \end{cases}. \quad (16)$$

The Riemann problem was chosen because it is one of the very few that have an analytical solution. This problem provides an excellent illustration of the wave nature of the equations. The solution to the Riemann problem is useful to verify the capturing of both smooth waves (characteristics) as well as non-smooth waves (shocks).

The initial states used were very similar to the Sod's[32] problem for Euler equations. They were:

$$\text{Left}: \begin{cases} \rho &= 1.0 \\ V_x &= 0.0 \\ V_y &= 0.0 \\ V_z &= 0.0 \\ B_x &= \frac{3}{4} \\ B_y &= 1.0 \\ B_z &= 0.0 \\ p &= 1.0 \end{cases} \quad \text{Right}: \begin{cases} \rho &= \frac{1}{8} \\ V_x &= 0.0 \\ V_y &= 0.0 \\ V_z &= 0.0 \\ B_x &= \frac{3}{4} \\ B_y &= -1.0 \\ B_z &= 0.0 \\ p &= \frac{1}{10} \end{cases}. \quad (17)$$

For a nondimensionalized form of the equations, the solution at at time $\tau = 0.1$ was computed, with the initial conditions described above. The solutions for the magnetic field and pressure profiles, with 400 points in the spatial dimension, are presented in figs. (6) and (7) respectively. The number of points in the domain, and the time τ were chosen to allow comparisons to other works, such as ref.[22].

In these figures, the fast rarefaction (FR) wave can be seen on the far right and the far left, as it is the fastest of the waves present in the problem. The slow

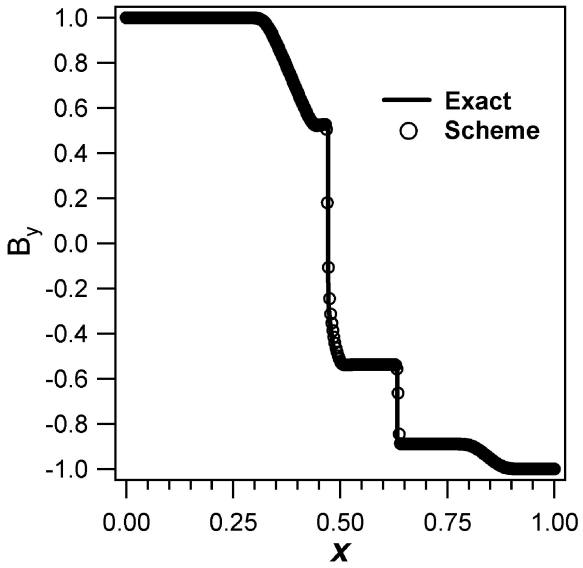

Figure 6: Magnetic field in the Riemann problem.

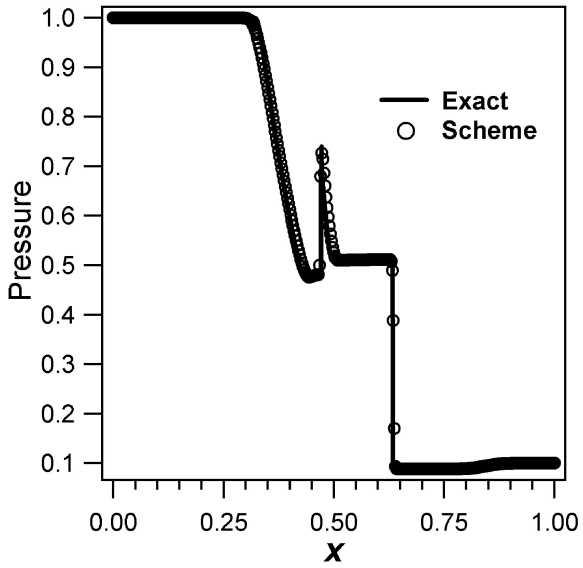

Figure 7: Pressure profile in the Riemann problem.

shock (SS) and the compound wave (SM) have speeds less than that of the FR wave.

As shown in these figures, the scheme successfully captures the time-dependent discontinuities.

5.2.2 Steady State Case

In order to simulate steady-state MHD flows, this solver can be used to solve the unsteady equation to steady state. Then, an important question is whether it remains in that steady state. To answer this question, a test problem was chosen, whose equilibrium solution is known analytically. This equilibrium solution is given as the initial condition for the solver. After marching several hundreds or thousands of time steps, a check is performed if the variables have changed from the initial conditions.

The test problem chosen for this simulation was the Taylor State[33] configuration. When a perfectly conducting plasma in an arbitrary initial condition is allowed to evolve, it will move quickly and dissipate energy before coming to rest. This stable equilibrium configuration can be analytically found using the minimum energy principle, and is of the form:

$$\nabla \times \mathbf{B} = \lambda \mathbf{B}, \tag{18}$$

where λ is an eigenvalue.

Since the current is parallel to the magnetic field, the $\mathbf{j} \times \mathbf{B}$ body force is identically zero. Furthermore, if there are no thermodynamic pressure gradients, the plasma is in a state of force-free equilibrium. For an axisymmetric geometry, the resulting magnetic field profile is:

$$B_\theta = B_0 J_1(\lambda r);\ B_z = B_0 J_0(\lambda r), \tag{19}$$

where B_o is a constant amplitude, J_0 and J_1 are Bessel functions of the first kind, of orders 0 and 1 respectively.

For a Cartesian grid of dimensions $L_x \times L_z$, with symmetry along the $\hat{y}$ direction, the magnetic field distribution satisfying eqn.(18) is:

$$\begin{aligned} B_x &= -\tfrac{B_0}{\sqrt{2}}\ \sin\left(\tfrac{m\pi x}{L_x}\right)\cos\left(\tfrac{n\pi z}{L_z}\right), \\ B_y &= B_0\ \sin\left(\tfrac{m\pi x}{L_x}\right)\sin\left(\tfrac{n\pi z}{L_z}\right), \\ B_z &= \tfrac{B_0}{\sqrt{2}}\ \cos\left(\tfrac{m\pi x}{L_x}\right)\sin\left(\tfrac{n\pi z}{L_z}\right), \end{aligned} \tag{20}$$

where m and n are eigenvalues.

With these initial conditions, the code was run for 10000 time steps on a 100×100 grid. At the end, the solution had deviated from equilibrium by less than 0.5%. The results from the code for B_x given in eqn.(20) are compared with the exact solution in Fig.(8).

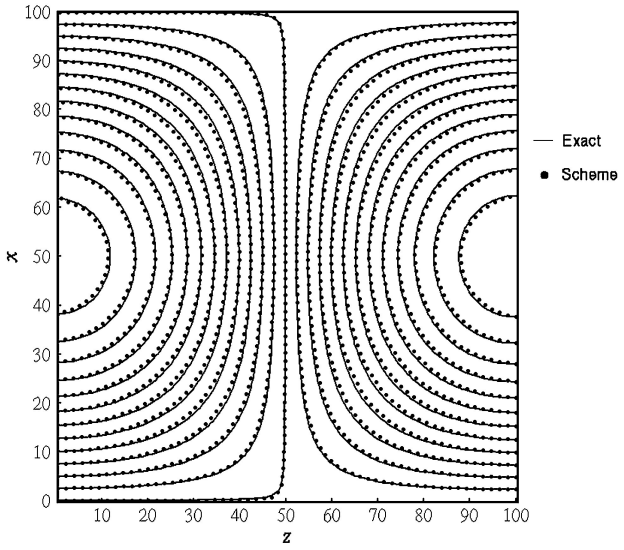

Figure 8: Magnetic field in the Taylor configuration

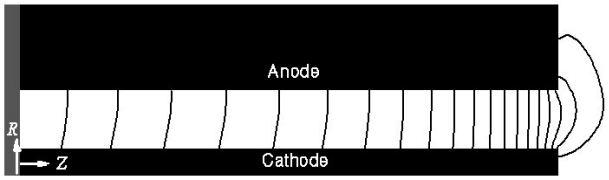

Figure 9: Current Lines in a coaxial thruster

6 Applications of the Scheme

The test cases described above were intended to validate the new characteristics splitting scheme, which was developed to calculate the convective part of the MHD equations. However, as described in sections 2 and 4, for the flows of interest both convection and diffusion are important. The ability of the numerical method to solve this mixed set of equations was tested by computing the flow of a resistive plasma in a coaxial self-field MPD thruster. Resistive diffusion was the only non-ideal MHD effect included in this computation. Other forms of dissipation, namely thermal conduction, viscosity and Joule heating were not included.

In the case chosen, the operating conditions were an external current of 6.0 kA, and Argon plasma at a mass flow rate of 6.0 g/s. The calculated contours of enclosed current at steady state are shown in Fig.(9). All the current is downstream of the backplate ($z = 0$), and there is 300 A of current flowing between each contour. In ideal MHD, magnetic field and therefore current lines, which are lines of constant rB_θ, would be convected to the exit. However, due to the presence of resistivity, the current lines remain in the channel. It is also apparent that many current lines inside the thruster are not vertical. This is because the Lorentz force is strongest near the cathode, and therefore magnetic convection is strongest there.

Though the contours in Fig.(9) look reasonable, they are not an accurate representation of a true MPD thruster flowfield. In order for the simulations to agree with experimental data, further refinements to the *physical* model are needed. As already mentioned, the physical model adapted to illustrate the scheme is simplistic. Specifically, the equations described above assume a fully ionized plasma, with ideal equation of state, in thermal equilibrium, and with only the classical form of transport coefficients, and lack the description of many energy sinks. Furthermore no sheath models are included. However, as stated above, such physical effects can be added without affecting the numerical foundation.

The extension to include the effect of two temperatures and finite ionization can be done in two steps:

1. Adding a continuity equation for electrons:

$$\frac{\partial \rho_e}{\partial t} + \nabla \cdot (\rho_e \mathbf{u}_e) = m_e \dot{n}_e, \tag{21}$$

   where $\dot{n}_e$ is the net ionization/recombination rate, and $\mathbf{u}_e = \mathbf{u} - \mathbf{j}/en_e$,

2. Adding a separate energy equation for electrons.

Including ionization reactions will bring in a different time scale to the problem, and the time-stepping scheme may have to change. However, this does not conflict with the methodology of the solver.

Another improvement that could be implemented easily is to include a realistic equation of state, as there is no fundamental change in the scheme to have $p/\rho = f(T)$.

Accurate expressions for classical transport coefficients, such as thermal conductivity and viscosity, and anomalous coefficients, obtained from ref. [11], can easily be introduced. These are presently being implemented in a code to simulate self-field MPD thrusters.

7 Concluding Remarks

A new solver to accurately compute plasma flows of interest to propulsion has been developed and validated. The characteristics-splitting technique is used to capture discontinuities monotonically. Flux-limited anti-diffusion to improve spatial accuracy away from discontinuities, and a multi-stage time stepping scheme to improve temporal accuracy are used in this numerical method. This solver has successfully demonstrated the capability to compute resistive plasma flows in simple geometries, thus showing promise to be a suitable platform to accurately simulate plasma thruster flows upon improvements in the physical model.

Acknowledgments The valuable advice of Prof. S. Jardin is sincerely appreciated.

References

[1] R.G. Jahn. *Physics of Electric Propulsion*. McGraw-Hill, 1968.

[2] J. E. Polk. *Mechanisms of Cathode Erosion in Plasma Thrusters*. PhD thesis, Princeton U., 1995.

[3] G. P. Sutton. *Rocket Propulsion Elements*. John Wiley, 1992.

[4] E. Y. Choueiri. *Advanced Problems in Plasma Propulsion*. Princeton U. Lecture Notes, 1998.

[5] H.C. Martinache. *A Theory on the Parallel-Plate Plasma Acceleration*. PhD thesis, Princeton U., 1974.

[6] D. D. Villani. *Energy Loss Mechanisms in a Magnetoplasmadynamics Arcjet*. PhD thesis, Princeton U., 1982.

[7] K. Toki I. Kimura and M. Tanaka. Current distribution on the electrodes of MPD arcjets. *AIAA J.*, 20(7):889, 1982.

[8] T.Ao and T. Fujiwara. Numerical and experimental study of an MPD thruster. *IEPC-84-08*, 1984.

[9] T. Miyasaka and T. Fujiwara. Numerical prediction of onset phenomenon in a 2-dimensional axisymmetric MPD thruster. *AIAA-99-2432*, 1999.

[10] G. Caldo. Numerical simulation of MPD thruster flows with anomalous transport. Master's thesis, Princeton University, 1994.

[11] E.Y. Choueiri. Anomalous resistivity and heating in current-driven plasma thrusters. *Phys. Plasmas*, 6(5):2290, 1999.

[12] M. LaPointe. Numerical simulation of geometric scale effects in cylindrical self-field MPD thrusters. *NASA-CR-189224*, 1992.

[13] J.M.G. Chanty and M. Martinez-Sanchez. Two-dimensional numerical simulation of MPD flows. *AIAA-87-1090*, 1987.

[14] E. H. Niewood. *An Explanation for Anode Voltage Drops in an MPD*. PhD thesis, MIT, 1993.

[15] P.J. Turchi, P.G. Mikellides, K.W. Hohman, R.J. Leiweke, I.G. Mikellides, C.S. Schmahl, N.F. Roderick, and R.E. Peterkin Jr. Progress in modeling plasma thrusters and related plasma flows. *IEPC-95-159*, 1995.

[16] D.C. Lilekis and R.E. Peterkin Jr. Effects of azimuthal injection asymmetry of MPD thruster performance using the MACH3 code. *IEPC-95-2677*, 1995.

[17] H.J. Kaeppeler C. Boie, M. Auweter-Kurtz and P.C. Sleziona. Application of adaptive numerical schemes for MPD thruster simulation. *IEPC-97-115*, 1997.

[18] J. Heiermann, M. Auweter-Kurtz, J. J. Kaeppeler, A. Eberle, U. Iben, and P. C. Sleziona. Recent improvements of numerical methods for the simulation of MPD thruster flow on adaptive meshes. *IEPC-99-169*, 1999.

[19] R. S. Myong. *Theoretical and Computational Investigation of Nonlinear Waves in Magnetohydrodynamics*. PhD thesis, U. Michigan, 1996.

[20] U. Shumlak, O. Jones, and S.D. Eberhardt. An implicit scheme for nonideal magnetohydrodynamics. *J. Comp. Phys*, 130:231, 1997.

[21] J.U. Brackbill and D.C. Barnes. The effect of nonzero $\nabla \cdot \mathbf{B}$ on the numerical solution of the magnetohydrodynamic equations. *J. Comp. Phys*, 35:426, 1980.

[22] K.G. Powell. An approximate Riemann solver for magnetohydrodynamics (that works in more than one dimension). *NASA ICASE Report 94-24*, 1994.

[23] L. Martinelli. *Calculations of Viscous Flows With a Multigrid Method*. PhD thesis, Princeton U., 1987.

[24] S.K. Godunov. Finite difference method for numerical computation of discontinous solution of the equations of fluid dynamics. *Matematicheskii Sbornik*, 47:15–21, 1959.

[25] S.K. Godunov. Symmetric form of the equations of magnetohydrodynamics. *Numerical Methods for Mechanics of Continuum Medium*, 1972.

[26] P. Roe. Approximate Riemann solvers, parameter vectors, and difference schemes. *J. Comp. Phys*, 43:357, 1981.

[27] P. Roe. Characteristics-based schemes for the Euler equations. *Annual Review of Fluid Mechanics*, 18:337, 1986.

[28] A. Jameson. Analysis and design of numerical schemes for gas dynamics, 1: Artificial diffusion, upwind biasing, limiters and their effect on accuracy and multigrid convergence. *Comp.Fluid.Dyn*, 1995.

[29] P. Cargo and G. Gallice. Roe matrices for ideal MHD and systematic construction of Roe matrices for systems of conservation laws. *J. Comp. Phys*, 136:446, 1997.

[30] K.G. Powell et al. An upwind scheme for magnetohydrodynamics. *AIAA-95-1704*, 1995.

[31] N. Aslan. Two-dimensional solutions of MHD equations with an adapted Roe method. *Int. J. Num. Meth. in Fluids*, 23(11):1211, 1996.

[32] G.A Sod. A survey of finite-difference methods for systems of nonlinear conservation laws. *J. Comp. Phys*, 27:1, 1978.

[33] J.B. Taylor. Relaxation of toroidal plasma and generation of reverse magnetic fields. *Physical Review Letters*, 1974.

[34] K.G. Powell et al. A solution-adaptive upwind scheme for ideal magnetohydrodynamics. *J. Comp. Phys*, 154:284–309, 1999.

A Eigensystem of MHD

Alfvèn speeds: $C_{A;r,\theta,z} = \frac{B_{r,\theta,z}}{\sqrt{\mu_o \rho}}$,

Sonic speed: $a = \sqrt{\frac{\gamma p}{\rho}}$

Normalization coefficients (based on the work in refs.[30], [34])

$$\beta_{r;\theta,z} = \frac{C_{A;\theta,z}}{\sqrt{C_{A;\theta}^2 + C_{A;z}^2}} \quad \alpha_{r;f,s} = \sqrt{\pm \frac{a^2 C_{S,F;r}^2}{C_{F;r}^2 - C_{S;r}^2}}$$
$$\beta_{z;r,\theta} = \frac{C_{A;r,\theta}}{\sqrt{C_{A;r}^2 + C_{A;\theta}^2}} \quad \alpha_{z;f,s} = \sqrt{\pm \frac{a^2 C_{S,F;z}^2}{C_{F;z}^2 - C_{S;z}^2}}$$

Fast and slow magnetosonic waves:

$$C_{F,S;\ r}^2 = \frac{1}{2}\left[(\frac{\mathbf{B}\cdot\mathbf{B}}{\mu_o \rho} + a^2) \pm \sqrt{(\frac{\mathbf{B}\cdot\mathbf{B}}{\mu_o \rho} + a^2)^2 - (4a^2 C_{A;\ r}^2)} \right]$$
$$C_{F,S;\ z}^2 = \frac{1}{2}\left[(\frac{\mathbf{B}\cdot\mathbf{B}}{\mu_o \rho} + a^2) \pm \sqrt{(\frac{\mathbf{B}\cdot\mathbf{B}}{\mu_o \rho} + a^2)^2 - (4a^2 C_{A;\ z}^2)} \right]$$

The Jacobian of transformation between primitive and conservation variables:

$$\frac{d\mathbf{U}}{d\mathbf{W}} = \begin{bmatrix} 1 & 0 & 0 & 0 & 0 & 0 & 0 & \\ u & \rho & 0 & 0 & 0 & 0 & 0 & 0 \\ v & 0 & \rho & 0 & 0 & 0 & 0 & 0 \\ w & 0 & 0 & \rho & 0 & 0 & 0 & 0 \\ 0 & 0 & 0 & 0 & 1 & 0 & 0 & 0 \\ 0 & 0 & 0 & 0 & 0 & 1 & 0 & 0 \\ 0 & 0 & 0 & 0 & 0 & 0 & 1 & 0 \\ \frac{\mathbf{u}\cdot\mathbf{u}}{2} & \rho u & \rho v & \rho w & \frac{B_x}{\mu_o} & \frac{B_y}{\mu_o} & \frac{B_z}{\mu_o} & \frac{1}{\gamma - 1} \end{bmatrix}$$

A.1 $\hat{\mathbf{r}}$ Direction

A.1.1 Eigenvalues

(in non-decreasing order):

$$\left[\ u - C_{F;r},\ u - C_{A;r},\ u - C_{S;r},\ u,\ u,\ u + C_{S;r},\ u + C_{A;r},\ u + C_{F;r}\ \right] \tag{22}$$

A.1.2 Ortho-normalized eigenvectors

$$L1_r = \left[0, \frac{-\alpha_{r;f} C_{F;r}}{2a^2}, \frac{\alpha_{r;s} C_{S;r} \beta_{r;\theta} Sgn[B_r]}{2a^2}, \frac{\alpha_{r;s} C_{S;r} \beta_{r;z} Sgn[B_r]}{2a^2}, 0, \frac{\alpha_{r;s} \beta_{r;\theta}}{2a\sqrt{\mu_o \rho}}, \frac{\alpha_{r;s} \beta_{r;z}}{2a\sqrt{\mu_o \rho}}, \frac{\alpha_{r;f}}{2\rho a^2}\right]$$
$$L2_r = \left[0, 0, -\frac{\beta_{r;z}}{\sqrt{2}}, \frac{\beta_{r;\theta}}{\sqrt{2}}, 0, -\frac{\beta_{r;z}}{\sqrt{2\mu_o \rho}}, \frac{\beta_{r;\theta}}{\sqrt{2\mu_o \rho}}, 0\right]$$
$$L3_r = \left[0, \frac{-\alpha_{r;s} C_{S;r}}{2a^2}, \frac{-\alpha_{r;f} C_{F;r} \beta_{r;\theta} Sgn[B_r]}{2a^2}, \frac{-\alpha_{r;f} C_{F;r} \beta_{r;z} Sgn[B_r]}{2a^2}, 0, \frac{-\alpha_{r;f} \beta_{r;\theta}}{2a\sqrt{\mu_o \rho}}, \frac{-\alpha_{r;f} \beta_{r;z}}{2a\sqrt{\mu_o \rho}}, \frac{\alpha_{r;f}}{2\rho a^2}\right]$$
$$L4_r = \left[1, 0, 0, 0, 0, 0, 0, 0, \frac{-1}{a^2}\right]$$
$$L5_r = [0, 0, 0, 0, 1, 0, 0, 0]$$
$$L6_r = \left[0, \frac{\alpha_{r;s} C_{S;r}}{2a^2}, \frac{\alpha_{r;f} C_{F;r} \beta_{r;\theta} Sgn[B_r]}{2a^2}, \frac{\alpha_{r;f} C_{F;r} \beta_{r;z} Sgn[B_r]}{2a^2}, 0, \frac{-\alpha_{r;f} \beta_{r;\theta}}{2a\sqrt{\mu_o \rho}}, \frac{-\alpha_{r;f} \beta_{r;z}}{2a\sqrt{\mu_o \rho}}, \frac{\alpha_{r;f}}{2\rho a^2}\right]$$
$$L7_r = \left[0, 0, -\frac{\beta_{r;z}}{\sqrt{2}}, \frac{\beta_{r;\theta}}{\sqrt{2}}, 0, \frac{\beta_{r;z}}{\sqrt{2\mu_o \rho}}, -\frac{\beta_{r;\theta}}{\sqrt{2\mu_o \rho}}, 0\right]$$
$$L8_r = \left[0, \frac{\alpha_{r;f} C_{F;r}}{2a^2}, \frac{-\alpha_{r;s} C_{S;r} \beta_{r;\theta} Sgn[B_r]}{2a^2}, \frac{-\alpha_{r;s} C_{S;r} \beta_{r;z} Sgn[B_r]}{2a^2}, 0, \frac{\alpha_{r;s} \beta_{r;\theta}}{2a\sqrt{\mu_o \rho}}, \frac{\alpha_{r;s} \beta_{r;z}}{2a\sqrt{\mu_o \rho}}, \frac{\alpha_{r;f}}{2\rho a^2}\right]$$

$$R1_r = \left[\rho\alpha_{r;f}, -\alpha_{r;f}C_{F;r}, \alpha_{r;s}C_{S;r}\beta_{r;\theta}Sgn\left[B_r\right], \alpha_{r;s}C_{S;r}\beta_{r;z}Sgn\left[B_r\right], 0, \alpha_{r;s}a\beta_{r;\theta}\sqrt{\mu_o\rho}, \alpha_{r;s}a\beta_{r;z}\sqrt{\mu_o\rho}, \rho a^2\alpha_{r;f}\right]$$
$$R2_r = \left[0, 0, \frac{-\beta_{r;z}}{\sqrt{2}}, \frac{\beta_{r;\theta}}{\sqrt{2}}, 0, \frac{-\beta_{r;z}\sqrt{\mu_o\rho}}{\sqrt{2}}, \frac{\beta_{r;\theta}\sqrt{\mu_o\rho}}{\sqrt{2}}, 0\right]$$
$$R3_r = \left[\rho\alpha_{r;s}, -\alpha_{r;s}C_{S;r}, -\alpha_{r;f}C_{F;r}\beta_{r;\theta}Sgn[B_r], -\alpha_{r;f}C_{F;r}\beta_{r;z}Sgn[B_r], 0, -\alpha_{r;f}a\beta_{r;\theta}\sqrt{\mu_o\rho}, -\alpha_{r;f}a\beta_{r;z}\sqrt{\mu_o\rho}, \rho a^2\alpha_{r;f}\right]$$
$$R4_r = [1, 0, 0, 0, 0, 0, 0, 0]$$
$$R5_r = [0, 0, 0, 0, 1, 0, 0, 0]$$
$$R6_r = \left[\rho\alpha_{r;s}, \alpha_{r;s}C_{S;r}, \alpha_{r;f}C_{F;r}\beta_{r;\theta}Sgn[B_r], \alpha_{r;f}C_{F;r}\beta_{r;z}Sgn[B_r], 0, -\alpha_{r;f}a\beta_{r;\theta}\sqrt{\mu_o\rho}, -\alpha_{r;f}a\beta_{r;z}\sqrt{\mu_o\rho}, \rho a^2\alpha_{r;f}\right]$$
$$R7_r = \left[0, 0, \frac{-\beta_{r;z}}{\sqrt{2}}, \frac{\beta_{r;\theta}}{\sqrt{2}}, 0, \frac{\beta_{r;z}\sqrt{\mu_o\rho}}{\sqrt{2}}, \frac{-\beta_{r;\theta}\sqrt{\mu_o\rho}}{\sqrt{2}}, 0\right]$$
$$R8_r = \left[\rho\alpha_{r;f}, \alpha_{r;f}C_{F;r}, -\alpha_{r;s}C_{S;r}\beta_{r;\theta}Sgn[B_r], -\alpha_{r;s}C_{S;r}\beta_{r;z}Sgn[B_r], 0, \alpha_{r;s}a\beta_{r;\theta}\sqrt{\mu_o\rho}, \alpha_{r;s}a\beta_{r;z}\sqrt{\mu_o\rho}, \rho a^2\alpha_{r;f}\right]$$

A.2 $\hat{z}$ Direction

A.2.1 Eigenvalues

(in non-decreasing order)

$$\left[\ w - C_{F;z},\ w - C_{A;z},\ w - C_{S;z},\ w,\ w,\ w + C_{S;z},\ w + C_{A;z},\ w + C_{F;z}\ \right] \tag{23}$$

A.2.2 Ortho-normalized eigenvectors

$$L1_z = \left[0, \frac{\alpha_{z;s}C_{S;z}\beta z;rSgn[B_z]}{2a^2}, \frac{\alpha_{z;s}C_{S;z}\beta_{z;\theta}Sgn[B_z]}{2a^2}, \frac{-\alpha_{z;f}C_{F;z}}{2a^2}, \frac{\alpha_{z;s}\beta_{z;r}}{2a\sqrt{\mu_o\rho}}, \frac{\alpha_{z;s}\beta z;\theta}{2a\sqrt{\mu_o\rho}}, 0, \frac{\alpha_{z;f}}{2\rho a^2}\right]$$
$$L2_z = \left[0, \frac{-\beta_{z;\theta}}{\sqrt{2}}, \frac{\beta_{z;r}}{\sqrt{2}}, 0, \frac{-\beta_{z;\theta}}{\sqrt{2\mu_o\rho}}, \frac{\beta_{z;r}}{\sqrt{2\mu_o\rho}}, 0, 0\right]$$
$$L3_z = \left[0, \frac{-\alpha_{z;f}C_{F;z}\beta z;rSgn[B_z]}{2a^2}, \frac{-\alpha_{z;f}C_{F;z}\beta_{z;\theta}Sgn[B_z]}{2a^2}, \frac{-\alpha_{z;s}C_{S;z}}{2a^2}, \frac{-\alpha_{z;f}\beta_{z;r}}{2a\sqrt{\mu_o\rho}}, \frac{-\alpha_{z;f}\beta z;\theta}{2a\sqrt{\mu_o\rho}}, 0, \frac{\alpha_{z;s}}{2\rho a^2}\right]$$
$$L4_z = [0, 0, 0, 0, 0, 0, 1, 0]$$
$$L5_z = \left[1, 0, 0, 0, 0, 0, 0, \frac{-1}{a^2}\right]$$
$$L6_z = \left[0, \frac{\alpha_{z;f}C_{F;z}\beta z;rSgn[B_z]}{2a^2}, \frac{\alpha_{z;f}C_{F;z}\beta_{z;\theta}Sgn[B_z]}{2a^2}, \frac{\alpha_{z;s}C_{S;z}}{2a^2}, \frac{-\alpha_{z;f}\beta_{z;r}}{2a\sqrt{\mu_o\rho}}, \frac{-\alpha_{z;f}\beta z;\theta}{2a\sqrt{\mu_o\rho}}, 0, \frac{\alpha_{z;s}}{2\rho a^2}\right]$$
$$L7_z = \left[0, \frac{-\beta_{z;\theta}}{\sqrt{2}}, \frac{\beta_{z;r}}{\sqrt{2}}, 0, \frac{\beta_{z;\theta}}{\sqrt{2\mu_o\rho}}, \frac{-\beta_{z;r}}{\sqrt{2\mu_o\rho}}, 0, 0\right]$$
$$L8_z = \left[0, \frac{-\alpha_{z;s}C_{S;z}\beta z;rSgn[B_z]}{2a^2}, \frac{-\alpha_{z;s}C_{S;z}\beta_{z;\theta}Sgn[B_z]}{2a^2}, \frac{\alpha_{z;f}C_{F;z}}{2a^2}, \frac{\alpha_{z;s}\beta_{z;r}}{2a\sqrt{\mu_o\rho}}, \frac{\alpha_{z;s}\beta z;\theta}{2a\sqrt{\mu_o\rho}}, 0, \frac{\alpha_{z;f}}{2\rho a^2}\right]$$

$$R1_z = \left[\rho\alpha_{z;f}, \alpha_{z;s}C_{S;z}\beta_{z;r}Sgn[B_z], \alpha_{z;s}C_{S;z}\beta_{z;\theta}Sgn[B_z], -\alpha_{z;f}C_{F;z}, \alpha_{z;s}a\beta_{z;r}\sqrt{\mu_o\rho}, \alpha_{z;s}a\beta_{z;\theta}\sqrt{\mu_o\rho}, 0, \rho a^2\alpha_{z;f}\right]$$
$$R2_z = \left[0, \frac{-\beta_{z;\theta}}{\sqrt{2}}, \frac{\beta_{z;r}}{\sqrt{2}}, 0, \frac{-\beta_{z;\theta}\sqrt{\mu_o\rho}}{\sqrt{2}}, \frac{\beta_{z;r}\sqrt{\mu_o\rho}}{\sqrt{2}}, 0, 0\right]$$
$$R3_z = \left[\rho\alpha_{z;s}, -\alpha_{z;f}C_{F;z}\beta_{z;r}Sgn[B_z], -\alpha_{z;f}C_{F;z}\beta_{z;\theta}Sgn[B_z], -\alpha_{z;s}C_{S;z}, -\alpha_{z;f}a\beta_{z;r}\sqrt{\mu_o\rho}, -\alpha_{z;f}a\beta_{z;\theta}\sqrt{\mu_o\rho}, 0, \rho a^2\alpha_{z;s}\right]$$
$$R4_z = [0, 0, 0, 0, 0, 0, 1, 0]$$
$$R5_z = [1, 0, 0, 0, 0, 0, 0, 0]$$
$$R6_z = \left[\rho\alpha_{z;s}, \alpha_{z;f}C_{F;z}\beta_{z;r}Sgn[B_z], \alpha_{z;f}C_{F;z}\beta_{z;\theta}Sgn[B_z], \alpha_{z;s}C_{S;z}, -\alpha_{z;f}a\beta_{z;r}\sqrt{\mu_o\rho}, -\alpha_{z;f}a\beta_{z;\theta}\sqrt{\mu_o\rho}, 0, \rho a^2\alpha_{z;s}\right]$$
$$R7_z = \left[0, \frac{-\beta_{z;\theta}}{\sqrt{2}}, \frac{\beta_{z;r}}{\sqrt{2}}, 0, \frac{\beta_{z;\theta}\sqrt{\mu_o\rho}}{\sqrt{2}}, \frac{-\beta_{z;r}\sqrt{\mu_o\rho}}{\sqrt{2}}, 0, 0\right]$$
$$R8_z = \left[\rho\alpha_{z;f}, -\alpha_{z;s}C_{S;z}\beta_{z;r}Sgn[B_z], -\alpha_{z;s}C_{S;z}\beta_{z;\theta}Sgn[B_z], \alpha_{z;f}C_{F;z}, \alpha_{z;s}a\beta_{z;r}\sqrt{\mu_o\rho}, \alpha_{z;s}a\beta_{z;\theta}\sqrt{\mu_o\rho}, 0, \rho a^2\alpha_{z;f}\right]$$